Title: AlphaFold predictions: great hypotheses but no match for experiment

Authors: Thomas C. Terwilliger[1,2]*, Dorothee Liebschner[3], Tristan I. Croll[4], Christopher J. Williams[5], Airlie J. McCoy[4], Billy K. Poon[3], Pavel V. Afonine[3], Robert D. Oeffner[4], Jane S. Richardson[5], Randy J. Read[4], and Paul D. Adams[3,6]

Affiliations:
[1]New Mexico Consortium, Los Alamos, NM 87544, USA

[2]Los Alamos National Laboratory, Los Alamos, NM 87545, USA

[3] Molecular Biophysics & Integrated Bioimaging Division, Lawrence Berkeley National Laboratory, Berkeley, CA 94720, USA.

[4]Department of Haematology, Cambridge Institute for Medical Research, University of Cambridge, Hills Road, Cambridge CB2 0XY, United Kingdom

[5]Department of Biochemistry, Duke University, Durham, North Carolina, 27710

[6]Department of Bioengineering, University of California, Berkeley, Berkeley, CA 94720, USA

*Corresponding author. Email: tterwilliger@newmexicoconsortium.org

Abstract: AI-based methods such as AlphaFold have raised the possibility of using predicted models in place of experimentally-determined structures. Here we assess the accuracy of AlphaFold predictions by comparing them to density maps obtained from automated redeterminations of recent crystal structures and to the corresponding deposited models. Some AlphaFold predictions match experimental maps closely, but most differ on a global scale through distortion and domain orientation and on a local scale in backbone and side-chain conformation. Such differences occur even in parts of AlphaFold models that were predicted with high confidence. Generally, the dissimilarities exceed those between high-resolution pairs of structures containing the same components but determined in different space groups. Therefore, while AlphaFold predictions are useful hypotheses about protein structures, experimental information remains essential for creating an accurate model.

One-Sentence Summary: AlphaFold predictions can be very accurate but should be treated as hypotheses as even high-confidence parts can be inconsistent with experimental data.

Main Text:

Protein structure predictions using AlphaFold (*1*), RoseTTAFold (*2*), and related methods (*3*) are far more accurate than previous generations of prediction algorithms (*4*), bringing much closer to reality the biological understanding derived from knowing the three-dimensional structures of all macromolecules (*1, 2, 5-8*). AlphaFold predictions have been made available for 200 million individual protein sequences to further drug discovery, protein engineering and understand biology (*9*). The question that immediately arises is whether these predictions can substitute for experimental structure determinations (*10*).

There is considerable discussion about limitations of AI-based models (*10, 11*). The accuracy of a prediction is typically assessed by how closely it matches a structure in the Protein Data Bank (*12*) (PDB) with the same sequence, but there are many ways to make such a comparison (*4*). Using comparisons that focus on local accuracy, predictions obtained with AlphaFold have been assessed as having "atomic accuracy" (*13*), as having accuracies competitive with "the best experimental results" (*4*) and being of comparable quality as an experimental crystal structure (*7*). It has been argued that AlphaFold predictions might be more accurate than estimated by comparison with models in the PDB, or even more accurate than the deposited models, because the deposited models are poorly defined in some places (*4*). This reasoning notes that side-chain positions and loops are sometimes not clear in crystallographic electron density maps(*14*), and in such cases a difference between an AlphaFold prediction and a deposited model would not indicate an error in the prediction. On the other hand, analyses carried out by the DeepMind team and others show that AlphaFold predictions vary substantially in their global and local agreement with deposited models and also in their coverage at the highest levels of confidence (*1, 10, 15*), with only about 40% of residues in the human proteome (*16*) modeled with high confidence.

Here we address the accuracy of AlphaFold predictions by assessing how well they agree with experimental data (*17*). We put these results into context by examining how closely one crystal structure in the PDB can typically be reproduced by another crystal structure containing the same components, but crystallized in a different space group (resulting in different crystal contacts).

Comparing AlphaFold models with crystallographic electron density maps

We used a set of crystallographic electron density maps determined without reference to deposited models as standards for evaluation of AlphaFold predictions. The density maps were obtained (*18*) using iterated AlphaFold prediction and model rebuilding with X-ray crystallographic data deposited in the PDB. For the present work we selected a high-quality subset of 102 models and maps from this analysis consisting of those that had free R values of 0.30 or better. The density maps in our analysis do not have any bias towards deposited models, as no information from deposited structures was used to compute these maps. Therefore, if features of a prediction are incompatible with the density maps and different from the deposited model, they are likely to be incorrect representations of the actual molecule in the crystal.

Fig. 1 compares AlphaFold predictions, experimental density maps, and corresponding deposited models (predictions were superimposed on the deposited models). All the residues shown in Fig. 1 were predicted with high confidence (pLDDT > 90) and the density maps range in resolution from 1.1 Å to 1.6 Å.

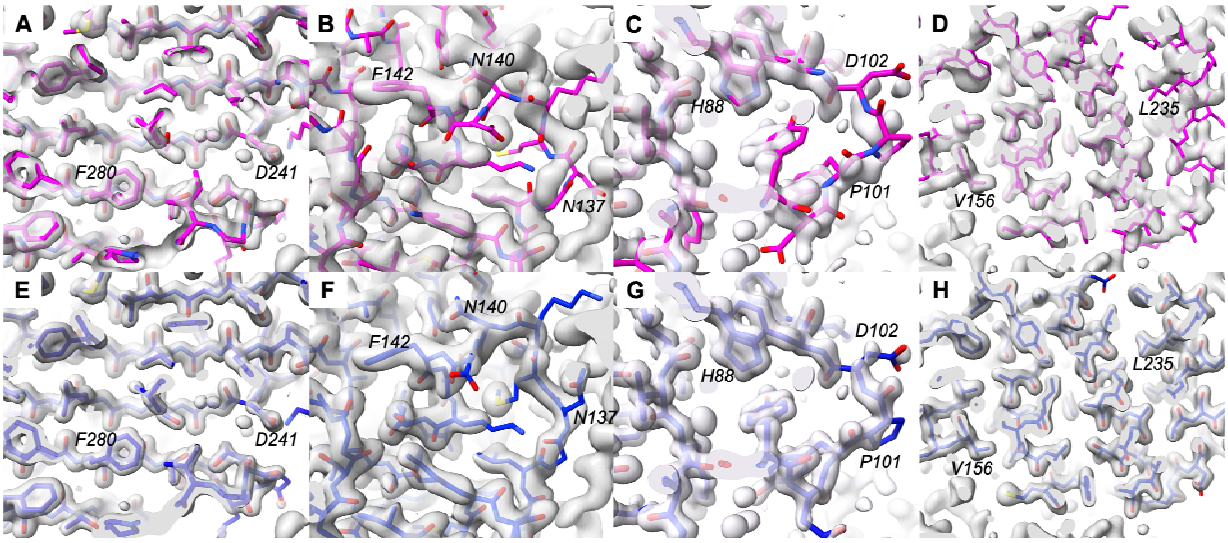

Figure 1. Comparison of details of AlphaFold predictions with density maps. AlphaFold predictions are shown in magenta with selected residues labeled; deposited models are shown in blue. Experimental electron density maps were taken from our previous work (*19*) and are contoured at 1.9 σ (**A**), (**E**), 1.1 σ (**B**), (**F**), 1.5 σ (**C**), (**G**), and 1.2 σ (**D**), (**H**). Model coloring is bright for parts of the models outside the density contours and dimmed for parts that are inside the contours. (A) and (E): PDB entry 7waa showing a region with high-accuracy prediction. (B) and (F): PDB entry 7s5L showing a region with incorrect prediction. (C) and (G): PDB entry 7t26 showing a prediction that does not match the density map, but where the density map is not fully clear. (D) and (H): PDB entry 7naz, showing a prediction that is distorted relative to the density map.

Figure 1A shows an example of an AlphaFold prediction that superimposes closely on the corresponding density map (PDB entry 7waa (*20*)). For comparison, Fig. 1E shows the deposited model along with the same density map. The overall map-model correlation for the superimposed AlphaFold prediction is 0.72 and the rms C_α difference from the deposited model is 0.5 Å.

Figure 1B shows a prediction for PDB entry 7s5L (*21*) which contained high-confidence regions that did not match the density map. The main chain corresponding to residues N137 through F142 match the density map poorly. In contrast, the deposited model matches the map very closely (Fig. 1F). The overall map-model correlation for the superimposed prediction is 0.44, much lower than that for the 7waa prediction shown in Fig. 1A, and the rms C_α difference from the deposited model is 2.1 Å.

Figure 1C shows an example of a prediction that does not match the density map but that might still represent a plausible conformation of the molecule. The prediction for PDB entry 7t26 (*22*) does not superimpose on the density near P101 and D102, while the deposited model does (Fig. 1G). The density map is less clear in this region than in other parts of the map. A break in main-chain density at D102 suggests that the chain adopts multiple conformations in this region. It is possible that the conformation in the AlphaFold prediction could be one of these alternative conformations, though not a dominant one as it does not appear in the density map.

Figure 1D illustrates a case where the AlphaFold prediction is distorted relative to the density map (PDB entry 7naz). Residues in the vicinity of V156 match the density closely (Fig. 1D), while residues near L235 are shifted relative to the map. For comparison, the deposited model matches the map closely throughout the region shown (Fig. 1H).

Figure 2A (open bars) shows the overall compatibility of 102 AlphaFold predictions with their corresponding density maps, as measured by map-model correlation. The mean map-model correlation for AlphaFold predictions (open bars) after superimposing them on corresponding deposited models was 0.56, substantially lower than the mean map-model correlation of deposited models to the same maps of 0.86 (hatched bars).

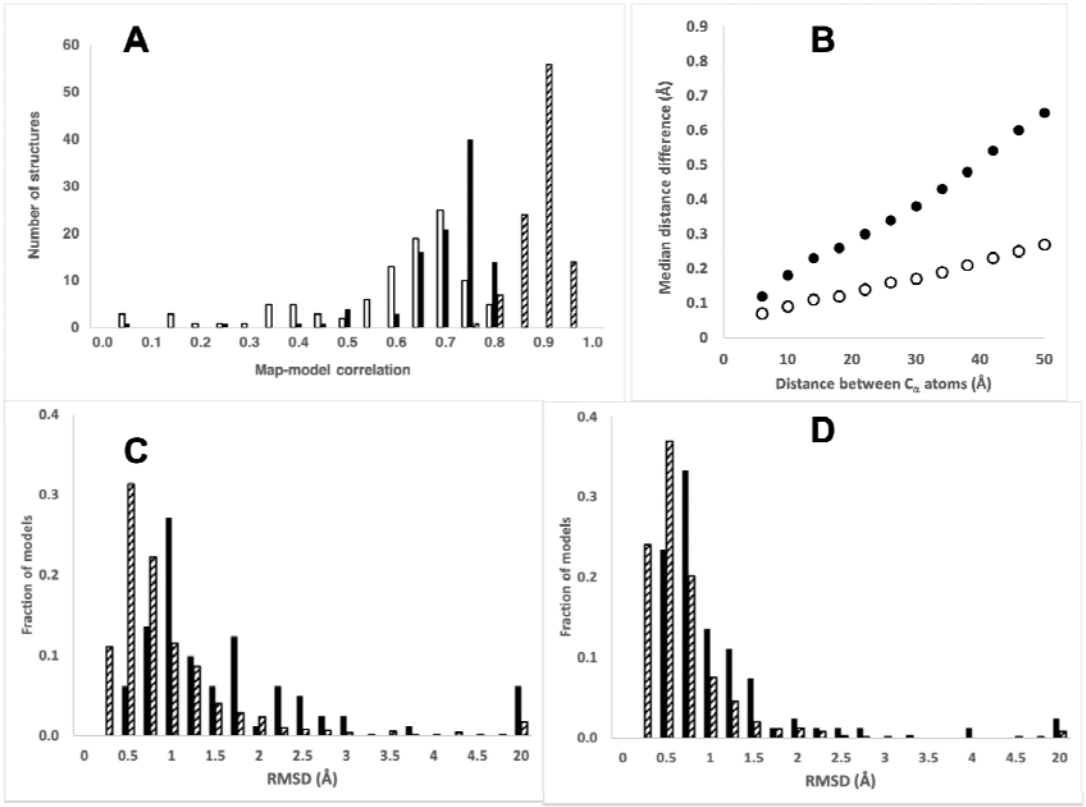

Figure 2. Overall comparison of AlphaFold predictions with density maps and deposited models. (**A**): Map-model correlation between 102 AlphaFold predictions (open bars), morphed AlphaFold predictions (solid bars), or corresponding deposited models (hatched bars) and experimental density maps. (**B**): Filled circles, median differences between distances in 102 AlphaFold models and those in corresponding deposited models, binned by the C_α - C_α distances (bin width of 4 Å). Open circles, as filled circles, but comparing matched pairs of structures from the PDB in which the components are the same but the crystal form is different. (**C**): RMSD between AlphaFold predictions and deposited models (solid bars) and between pairs of matching PDB entries with the same composition (hatched bars). The category at the far right on the abscissa labelled "20" includes all values greater than 5 Å. (**D**): As in C except after morphing models to match.

Distortion and domain movement in AlphaFold predictions

Figure 1D illustrated that an AlphaFold prediction can be somewhat distorted relative to the actual structure. To determine whether this occurs for many AlphaFold predictions, we "morphed" each AlphaFold prediction to make it more similar to the deposited model (see Materials and Methods). This process reduces differences between predictions and deposited models that arise from either distortion or alternate locations of domains within chains. After morphing each predicted model, the predictions agree more closely with the electron density maps (Fig. 2A, solid bars, mean map correlation of 0.67 vs 0.56 before morphing), but still much less closely than the deposited models (Fig. 2A, hatched bars, mean map correlation of 0.86).

If two models are related by a long-range distortion or alternate locations of domains, inter-atomic distances that are short will be similar in the two models, while those that are long will differ. We quantified this relationship by comparing inter-atomic distances in predicted models with matching distances in deposited models and examining the median differences as a function of distance. Fig. 2B shows that this median inter-atomic distance deviation between deposited models and moderate-to-high-confidence parts of AlphaFold predictions (pLDDT above 70) is about 0.1 Å for atom pairs that are close (between 4 Å and 8 Å apart) and increases to 0.7 Å for distant atom pairs (48 Å – 52 Å), indicating a typical distortion of about 0.5-1 Å over this range of distances. As a reference, we analyzed 926 pairs of high-resolution structures in the PDB that had identical sequences but were obtained in different crystallographic space groups (so that crystal contacts influencing conformation would differ). Fig. 2B shows that atom pairs in these matching structures had distances that differed by a rms of 0.1 Å for nearby residues and 0.4 Å for distant ones, about half the values found for AlphaFold predictions.

As a third method of assessing distortion and differences in domain relationships in AlphaFold predictions, we compared them with the corresponding models from the PDB, calculating the rmsd of C_α atoms both before and after applying the distortion field described above. For this analysis we used all 215 structures analyzed in our previous work (*19*). Fig. 2C shows the distribution of C_α rmsd values for the AlphaFold predictions; the median rmsd is 1.0 Å. After applying the distortion field, the median rmsd is reduced to 0.4 Å (Fig. 2D, the median rsmd distortion applied was 0.6 Å). For matching pairs of structures in the PDB crystallized in different space groups, the median C_α rmsd was only 0.6 Å, and this could be reduced to 0.4 Å by applying a distortion field (median rms distortion applied of 0.2 Å). Overall, the C_α coordinates in AlphaFold predictions are considerably more different from PDB entries than deposits of high-resolution structures of the same molecule in different space groups are from each other (median rmsd of 1.0 Å vs 0.6 Å), and a substantial part of this difference consists of long-range distortion.

Comparing AlphaFold side-chain predictions with experimental density maps

As illustrated in Fig. 1, AlphaFold predictions often contain at least some regions that are similar to deposited structures, but even in these regions many details often differ. We used the 102 electron density maps described above along with deposited models to evaluate side-chain conformations (the locations of atoms in side-chains relative to the atoms in the main-chain that they are connected to), an important local feature of a structural model. In order to analyze the local side-chain structure and remove confounding effects from domain shifts or distortions, we grafted the side-chain from each residue in an AlphaFold prediction onto the corresponding main-chain atoms residue of the deposited model. This yielded a composite model with the main-chain coordinates of the deposited models and side-chain conformations corresponding to the AlphaFold predictions.

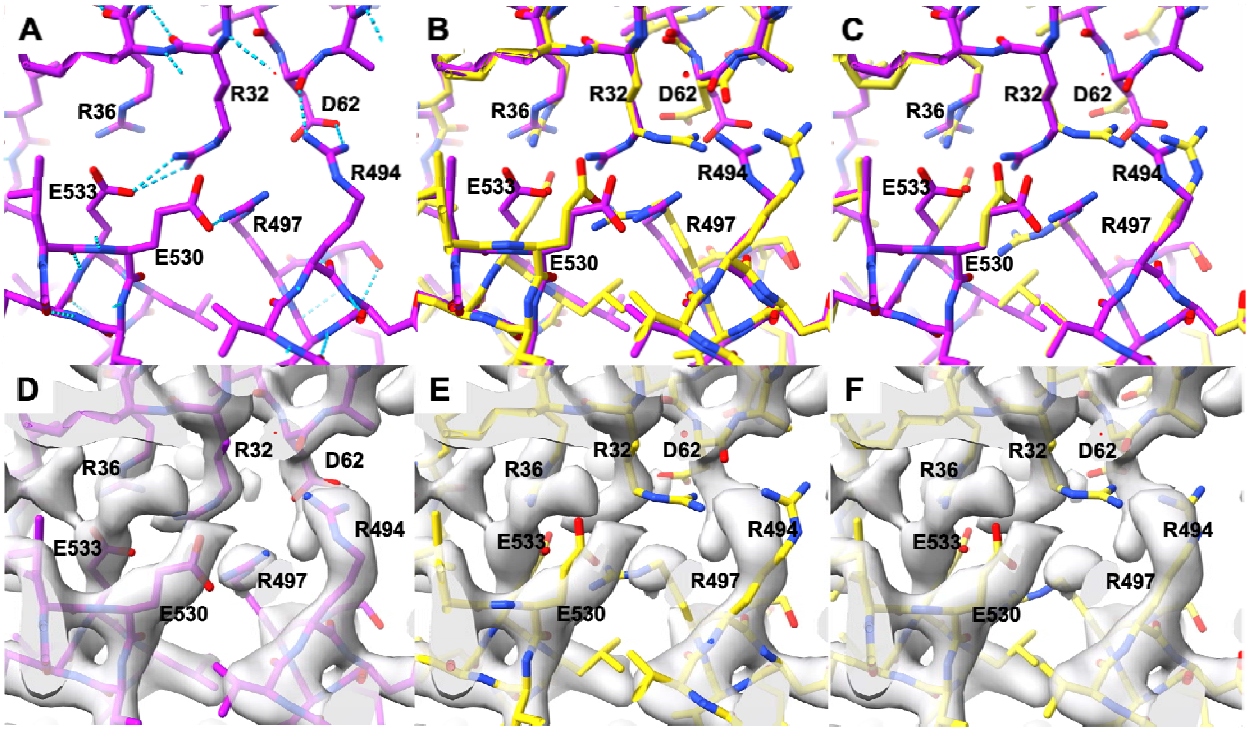

Figure 3. Comparison of AlphaFold side-chain predictions with density map for PDB entry 7vgm. (**A**): PDB entry 7vgm showing hydrogen bonding network. (**B**): AlphaFold prediction (yellow) superimposed on deposited model for PDB entry 7vgm (magenta). (**C**): As in B, except the AlphaFold side-chains (yellow) are grafted on to the backbone for PDB entry 7vgm (main-chain atoms for each model are used to superimpose the side-chains). (**D**): Deposited model as in A superimposed on experimental density map (2.3 Å resolution). (**E**): AlphaFold prediction as in B superimposed on density map. (**F**): grafted AlphaFold model superimposed on density map.

Figure 3A shows a local portion of PDB entry 7vgm, and Fig. 3B shows the AlphaFold prediction superimposed on the deposited model. Fig 3C shows the same region with the grafted side-chain and the composite model. The positions of several of the side-chains in the AlphaFold model (e.g., R32, D62, E530, E533, R494) are different from those in the deposited model. Fig. 3D shows the deposited model for 7vgm along with the density map obtained for PDB entry 7vgm, and Fig. 3E shows the AlphaFold model superimposed on the same density map. Even though the density map was obtained with the AlphaFold prediction and without reference to the deposited model, all the side-chains in the deposited model match the map closely. In contrast, side-chains in the AlphaFold prediction that were different from those in the deposited model do not match the density map, both before (Fig. 3E) and after (Fig. 3F) grafting, indicating that these side-chain conformations are likely to be incorrect.

We carried out this side-chain grafting procedure for 102 AlphaFold predictions and the corresponding deposited models. For each pair of side-chains, we examined the agreement between atomic positions in that side-chain and the corresponding optimized density map. We identified pairs in which the AlphaFold side-chain prediction differed substantially from the deposited model (rmsd of side-chain atoms > 1.5 Å). Then based on estimates of the uncertainty of density values in each map and of the number of independent points sampled by side-chain atomic positions in that map, we identified AlphaFold side-chain predictions that differed from the deposited model and were highly unlikely ($p < 0.01$) to be as compatible with the density

map as the deposited model. We considered these AlphaFold side-chain predictions to be incompatible with the experimental data.

Overall, we found that 20% of the side-chains in moderate-to-high confidence residues of AlphaFold predictions and not involved in crystal contacts had different conformations than in the corresponding deposited model (at least 1.5 Å rmsd), and one third of these (7% overall) were clearly incompatible with the experimental data. As the number of clearly-incompatible residues identified by our method is a lower estimate, we expect that the actual level of disagreement between AlphaFold predictions and conformations of the molecules in the crystals is somewhere between the 7% that are clearly incompatible with the data and the 20% that differ from the deposited models.

To put the fraction of side-chain positions in AlphaFold predictions that are incompatible with the experimental data into perspective, we carried out a similar analysis, but using the set of high-resolution structures from the PDB containing the same components but crystallized in a different space group. For these tests we used experimentally-based density maps (2mFo-DFc maps (*23*) calculated using one model from each pair. Here, only 6% of the side-chains differed by 1.5 Å rmsd, and only 2% were in conformations that were experimentally incompatible with the corresponding conformations from the other set. Therefore, at a detailed level as well as an overall level, the differences between AlphaFold predictions and these crystal structures are substantially greater than for pairs of crystal structures determined in different space groups.

We then analyzed whether the 7% of residues in AlphaFold predictions that were incompatible with experimental data included residues with functional significance. We extracted all the residues that were explicitly mentioned in the 49 publications describing the 102 analyzed structures, yielding a total of 733 named residues. Of these, 53 (7%) were among the residues we identified as being incompatible with experimental data, the same percentage that we found for all residues. For example, residues R32, D62, R497 and E533 in Fig. 3 are all in this group of functional residues that are incompatible with experimental data.

As functionally significant residues are constrained by evolution it might have been expected that the evolutionary covariation that forms a central element of AlphaFold prediction (*13*) would be stronger than average. On the other hand, these same residues are more conserved than average (*24*), possibly balancing that effect. In our small sample, we do not see a substantial effect either way, rather we find that side-chains for residues in AlphaFold predictions with functional significance are about as likely to be incompatible with experimental data as other side-chains.

Using confidence (pLDDT) to estimate errors in AlphaFold predictions

As AlphaFold predictions can differ substantially from corresponding experimental models, straightforward methods to estimate coordinate uncertainties of these predictions would be useful. As a first step, we superimposed AlphaFold predictions on corresponding deposited models and determined the distance between the C_α atoms in the predicted and deposited models, as well as the confidence (pLDDT) for the predicted C_α atom.

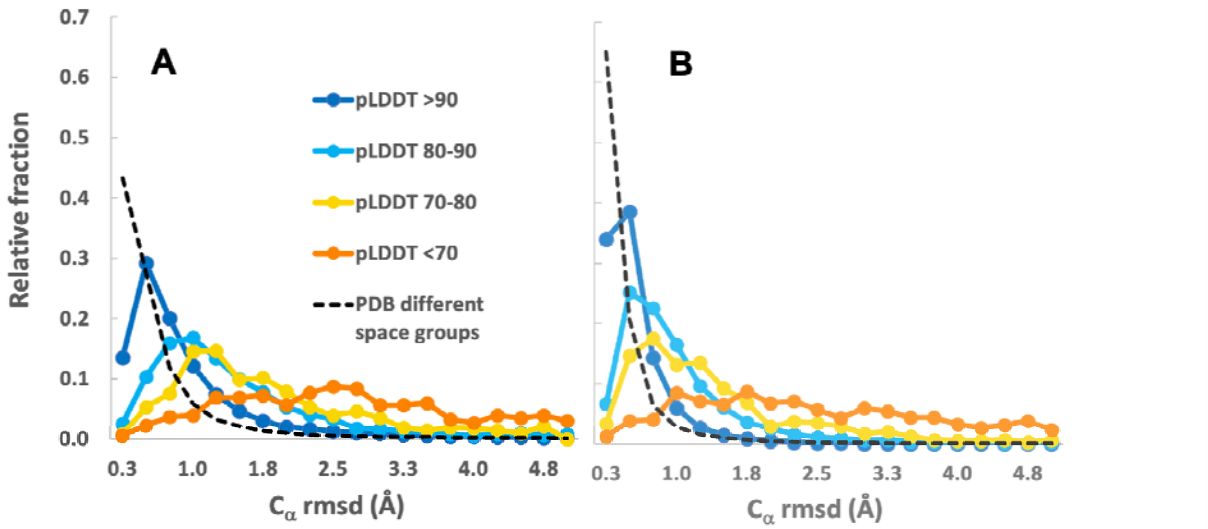

Figure 4. Distribution of prediction errors for ranges of AlphaFold prediction confidence. Dark blue dots and line, pLDDT > 90, light blue, between 80 and 90, yellow, between 70 and 80, orange, less than 70. Ordinate is the fraction of cases in the ranges of rmsd indicated on the abscissa. Dashed line shows similar comparison for matching pairs of PDB deposits with different space groups. (**A**): errors estimated for structures as is. (**B**): Errors estimated after morphing.

Figure 4A shows the distribution of prediction errors for various ranges of the confidence measure. For comparison, the dashed line in Fig. 4A shows the distribution of differences between matching C_α atoms in pairs of structures containing the same components but crystallized in different space groups. The median prediction error for high-confidence (pLDDT > 90) residues was 0.6 Å, while for residues with pLDDT between 80 and 90 it was 1.1 Å, and for those between 70 and 80 it was 1.5 Å (Table I). By comparison, matching C_α atoms in pairs of structures in different space groups differed by a median of 0.3 Å. Fig. 4B shows that morphing one member of each pair as described above reduces the differences over all confidence ranges, but differences between matching pairs of structures in the PDB are reduced similarly.

AlphaFold confidence (pLDDT)	Median prediction error (Å)	Percentage with error over 2 Å
>90	0.6	10
80 - 90	1.1	22
70 - 80	1.5	33
<70	3.5	77

Table I. Median prediction error and percentage with prediction error over 2 Å by AlphaFold confidence.

We note these distributions do not resemble the expected Maxwell-Boltzmann distribution for 3-dimensional Gaussian errors (excess kurtosis of over 200 for errors in prediction vs an expected value of 0.1). The distributions have a small fraction of values that are very large (long tails in the distributions), so describing uncertainties in terms of rms errors may not ordinarily be effective. Instead, it may be more useful to note the median errors described above as a measure of typical errors, and to also take into account the percentage of instances where the error is very large (i.e., completely wrong). The definition of very large errors will depend on the situation,

but often atomic positions that deviate by more than 2 or 3 Å are of limited value. For the structures analyzed here, about 10% of C_α atoms with pLDDT over 90 are found to be in error by over 2 Å, along with 22% of those with pLDDT between 80 and 90, 33% of those between 70 and 80, and 77% of those with pLDDT under 70 (Table I). For comparison, just 5% of C_α atoms in the matched pairs of structures in the PDB crystallized in different space groups we analyzed differ by over 2 Å.

The lack of agreement between AlphaFold predictions and experimental data is consistent with results of the uncertainty quantification carried out by DeepMind during the development of AlphaFold (*25*). That analysis estimated that 7% (for pLDDT > 90) to 30% (for 70 < pLDDT < 90) of side-chains have a χ_1 angle deviation of at least 40^o. Such a deviation typically leads to an rmsd of side-chain atoms of over 1.5 Å. In our analysis, the average pLDDT was 94, with 12% of residues having a pLDDT between 70 and 90. Therefore, the errors estimated in AlphaFold development are generally consistent with our observation that between 7% and 20% of side-chains with pLDDT of 70 or above are incompatible with experimental data.

Conclusions

While some AlphaFold predictions are astonishingly accurate (e.g., Fig 1A), we find that many parts of these predictions are incompatible with experimental data from corresponding crystal structures. In particular, our results show that AlphaFold predictions are not better representations of the contents of a crystal than the models deposited in the PDB, as the deposited models agree much more closely with experimental data where the predicted and deposited models differ. Our results also show that AlphaFold predictions differ from corresponding models deposited in the PDB by much more than pairs of high-resolution structures in the PDB that were crystallized in different space groups, indicating that AlphaFold predictions are in error by more than the amount that might be expected due to flexibility. We conclude that while AlphaFold models are good hypotheses for protein structures, they have major limitations.

Despite their limitations, AlphaFold predictions are already changing the way that hypotheses about protein structures are generated and tested (*1, 2, 5, 6*). Indeed, even though not all parts of AlphaFold predictions are accurate, they provide plausible hypotheses that can suggest mechanisms of action and allow designing experiments with specific expected outcomes. Using these predictions as starting hypotheses can also greatly accelerate the process of experimental structure determination (*18, 26, 27*). AlphaFold predictions often have very good stereochemical characteristics, making them excellent hypotheses for local structural features. For example, for the 102 structures analyzed here, the mean percentage of residues with “favored” Ramachandran configurations was 98%, greater than that of the corresponding deposited models (97%), and the mean percentage of side-chain conformations classified as outliers was just 0.2%, compared with 1.5% for deposited models (*19*). Such AlphaFold predictions with highly plausible geometry could be used in later stages of experimental structure determination as potential conformations for segments of structure that are not fully clear in experimental density maps.

References and Notes

1. J. Jumper *et al.*, Highly accurate protein structure prediction with AlphaFold. *Nature* **596**, 583-589 (2021).

2. M. Baek *et al.*, Accurate prediction of protein structures and interactions using a three-track neural network. *Science* **373**, 871-876 (2021).
3. Z. Lin *et al.*, Evolutionary-scale prediction of atomic level protein structure with a language model. *bioRxiv*, 2022.2007.2020.500902 (2022).
4. A. Kryshtafovych, T. Schwede, M. Topf, K. Fidelis, J. Moult, Critical assessment of methods of protein structure prediction (CASP)—Round XIV. *Proteins: Structure, Function, and Bioinformatics* **89**, 1607-1617 (2021).
5. E. Callaway, 'The entire protein universe': AI predicts shape of nearly every known protein. *Nature* **608**, 15-16 (2022).
6. J. M. Thornton, R. A. Laskowski, N. Borkakoti, AlphaFold heralds a data-driven revolution in biology and medicine. *Nature Medicine* **27**, 1666-1669 (2021).
7. M. van Breugel, I. Rosa e Silva, A. Andreeva, Structural validation and assessment of AlphaFold2 predictions for centrosomal and centriolar proteins and their complexes. *Communications Biology* **5**, 312 (2022).
8. S. Subramaniam, G. J. Kleywegt, A paradigm shift in structural biology. *Nature Methods* **19**, 20-23 (2022).
9. D. Hassabis. https://www.deepmind.com/blog/alphafold-reveals-the-structure-of-the-protein-universe
10. C. Shao, S. Bittrich, S. Wang, S. K. Burley, Assessing PDB macromolecular crystal structure confidence at the individual amino acid residue level. *Structure*, (2022).
11. P. B. Moore, W. A. Hendrickson, R. Henderson, A. T. Brunger, The protein-folding problem: Not yet solved. *Science* **375**, 507 (2022).
12. H. M. Berman *et al.*, The Protein Data Bank. *Nucleic Acids Res* **28**, 235-242 (2000).
13. J. Jumper, D. Hassabis, Protein structure predictions to atomic accuracy with AlphaFold. *Nature Methods* **19**, 11-12 (2022).
14. B. van Beusekom, K. Joosten, M. L. Hekkelman, R. P. Joosten, A. Perrakis, Homology-based loop modeling yields more complete crystallographic protein structures. *IUCrJ* **5**, 585-594 (2018).
15. C. F. Hryc, M. L. Baker, AlphaFold2 and CryoEM: Revisiting CryoEM modeling in near-atomic resolution density maps. *iScience* **25**, 104496 (2022).
16. E. Porta-Pardo, V. Ruiz-Serra, S. Valentini, A. Valencia, The structural coverage of the human proteome before and after AlphaFold. *PLOS Computational Biology* **18**, e1009818 (2022).
17. T. G. Flower, J. H. Hurley, Crystallographic molecular replacement using an in silico-generated search model of SARS-CoV-2 ORF8. *Protein Science* **30**, 728-734 (2021).
18. T. C. Terwilliger *et al.*, Improved AlphaFold modeling with implicit experimental information. *Nature Methods*, (2022).
19. T. C. Terwilliger *et al.*, Accelerating crystal structure determination with iterative AlphaFold prediction. *bioRxiv*, 2022.2011.2018.517112 (2022).
20. Q. Zhang *et al.*, Re-sensitization of mcr carrying multidrug resistant bacteria to colistin by silver. *Proc Natl Acad Sci U S A* **119**, e2119417119 (2022).
21. I. Burkhardt, T. de Rond, P. Y.-T. Chen, B. S. Moore, Ancient plant-like terpene biosynthesis in corals. *Nature Chemical Biology* **18**, 664-669 (2022).
22. S. J. Hobbs *et al.*, Phage anti-CBASS and anti-Pycsar nucleases subvert bacterial immunity. *Nature* **605**, 522-526 (2022).
23. R. Read, Improved Fourier coefficients for maps using phases from partial structures with errors. *Acta Crystallographica Section A* **42**, 140-149 (1986).

24. G. J. Bartlett, C. T. Porter, N. Borkakoti, J. M. Thornton, Analysis of Catalytic Residues in Enzyme Active Sites. *Journal of Molecular Biology* **324**, 105-121 (2002).
25. K. Tunyasuvunakool *et al.*, Highly accurate protein structure prediction for the human proteome. *Nature* **596**, 590-596 (2021).
26. A. J. McCoy, M. D. Sammito, R. J. Read, Implications of AlphaFold2 for crystallographic phasing by molecular replacement. *Acta Crystallographica Section D* **78**, 1-13 (2022).
27. I. Barbarin-Bocahu, M. Graille, The X-ray crystallography phase problem solved thanks to AlphaFold and RoseTTAFold models: a case-study report. *Acta Crystallogr D Struct Biol* **78**, 517-531 (2022).
28. R. D. Oeffner *et al.*, Putting AlphaFold models to work with phenix.process_predicted_model and ISOLDE. *Acta Crystallographica Section D* **78**, (2022).
29. T. Terwilliger, Maximum-likelihood density modification. *Acta Crystallographica Section D* **56**, 965-972 (2000).
30. K. Cowtan, S. Metcalfe, P. Bond, Shift-field refinement of macromolecular atomic models. *Acta Crystallographica Section D* **76**, 1192-1200 (2020).
31. P. V. Afonine *et al.*, Towards automated crystallographic structure refinement with phenix.refine. *Acta Crystallographica Section D* **68**, 352-367 (2012).
32. I. W. Davis, W. B. Arendall, D. C. Richardson, J. S. Richardson, The Backrub Motion: How Protein Backbone Shrugs When a Sidechain Dances. *Structure* **14**, 265-274 (2006).
33. R. Evans *et al.*, Protein complex prediction with AlphaFold-Multimer. *bioRxiv*, 2021.2010.2004.463034 (2022).
34. M. J. Bennett, S. Choe, D. Eisenberg, Domain swapping: entangling alliances between proteins. *Proc Natl Acad Sci U S A* **91**, 3127-3131 (1994).

Acknowledgments:

Funding:

Lawrence Berkeley National Laboratory grant DE-AC02-05CH11231 (PDA)

National Institutes of Health grant GM063210 (PDA, JSR, RJR, TCT)

Wellcome Trust grant 209407/Z/17/Z (RJR)

Phenix Industrial Consortium (PDA)

Author contributions:

Conceptualization: TCT, PDA, RJR, JSR

Methodology: TCT, PDA, RJR, JSR

Investigation: TCT, AJM, BKP, PVA, TIC, CJW, DL, RDO

Visualization: TCT

Funding acquisition: TCT, PDA, RJR, JSR

Project administration: TCT, PDA, RJR, JSR

Supervision: TCT, PDA, RJR, and JSR

Writing – original draft: TCT

Writing – review & editing: TCT, PDA, RJR, JSR, AJM, BKP, PVA, TIC, CJW, DL, RDO

Competing interests: None

Data and materials availability: Input data for deposited models were taken from the Protein Data Bank. The 102 accession codes used were: 7e0m, 7fhr, 7v6p, 7Ljh, 7p3a, 7v38, 7v3b, 7o9p, 7rLz, 7qdv, 7ewj, 7rw4, 7waa, 7kdx, 7fiu, 7n3v, 7ptb, 7dtr, 7aoj, 7rc2, 7tcr, 7wja, 7vnx, 7x8v, 7raw, 7rpy, 7aov, 7tb5, 7t8L, 7vwk, 7ne9, 7nqd, 7s5L, 7wbk, 7x77, 7e3z, 7f0o, 7v1q, 7etx, 7ety, 7ecd, 7dxn, 7eyj, 7e4d, 7wsj, 7fi3, 7wnn, 7vgm, 7eio, 7v9n, 7tvc, 7Lbk, 7e6v, 7b3n, 7bLL, 7djj, 7dms, 7dqx, 7drh, 7dri, 7e1d, 7e85, 7edc, 7ejg, 7es4, 7esi, 7eus, 7ew8, 7exx, 7f2a, 7fjg, 7kzh, 7Lsv, 7mku, 7naz, 7ncy, 7nxg, 7o51, 7o5y, 7oc3, 7oom, 7oq6, 7qs4, 7rm7, 7t7j, 7tbs, 7tem, 7tfq, 7tj1, 7tL5, 7tmu, 7tog, 7toj, 7trv, 7trw, 7tt9, 7twc, 7tzp, 7unn, 7w3s, 7wdq, 8cuk. All models are downloadable from the PDB with links such as: https://files.rcsb.org/download/7tzp.pdb or (for larger models that are not available in this format) https://files.rcsb.org/download/7tzp.cif . We used the Phenix tool *fetch_pdb* to download models and crystallographic data for each structure. Predicted models, rebuilt models, and density-modified map coefficients are available at: https://phenix-online.org/phenix_data/terwilliger/alphafold_crystallography_2022/ along with a spreadsheet that contains all the raw data and analyses described in our previous work (*19*) and described here. The directory terwilliger/alphafold_crystallography_2022/ contains a README file describing the contents of the site, the spreadsheet, and a data/ directory with one compressed archive for each structure containing models and crystallographic data files. This directory also contains a compressed archive (*alphafold_crystallography.tgz*) containing all the data and all the scripts used to create the spreadsheet.

Code Availability: All code for the Phenix version of the AlphaFold2 Colab is freely available on GitHub at https://github.com/phenix-project/Colabs. All code for Phenix is available at phenix-online.org.

Supplementary Materials

Materials and Methods

Experimental data, models, AlphaFold predictions, and density maps

We used the results of our automated structure redeterminations (*19*) for crystallographic PDB deposits in this work. The structures in that study were chosen based on the method of structure solution (single-wavelength anomalous diffraction, SAD), used as a proxy for relatively challenging structure determinations. The anomalous data were not used in our structure redeterminations, i.e., the Bijvoet pairs were averaged. All the unique, protein-containing structures in a 6-month period (Dec. 2021-May 2022) were analyzed (215 structures). Structures were determined with molecular replacement using trimmed AlphaFold predictions (*28*) as search models, followed by iterative model rebuilding and AlphaFold prediction (*18*). In this work we use the initial AlphaFold predictions (made without templates) and the final density-modified electron density maps (*29*) from those analyses. Except as noted, in this work we used only structures yielding a free R value of 0.30 or lower (102 structures) to ensure that the density-modified electron density maps used as a reference were of high quality.

Model morphing with a distortion field

We used a morphing procedure based on a smoothed distortion field (*30*) to modify one model to make it globally more similar to another model, while retaining local differences. In this procedure any point in space has an associated shift vector, the shift that is to be applied to any atom located at that point in space. This association of a vector to each point in space amounts to a shift or distortion field. To create a smoothly-varying distortion field relating a pair of structures, we first create an exact distortion field that maps one structure onto the other, then this field is smoothed.

First, the two structures are superimposed. Then a set of positions in space and corresponding shift vectors is created, with the positions in space $\boldsymbol{y}_i$ corresponding to C_α atom coordinates in one structure, and the shift vectors $\boldsymbol{v}_i$ corresponding to the differences between matching C_α atoms in the two structures. At this point, each of these positions in space has the property that if the associated shift vector is added, it will match the corresponding C_α atom coordinate in the other structure. This exact distortion field is defined only at the C_α atom coordinates of the first structure.

Then we create a smoothed distortion field $\boldsymbol{v(x)}$ that is defined at any point in space $\boldsymbol{x}$ by averaging all the shift values in the exact distortion field, weighting individual shifts $\boldsymbol{v}_i$ with a weight $\boldsymbol{w}_i$ based on the distances between their positions in space $\boldsymbol{y}_i$ and that point $\boldsymbol{x}$,

$$\boldsymbol{w}_i = exp(-||\boldsymbol{y}_i - \boldsymbol{x}||^2/u^2),$$

where the scaling factor u determines the distance over which smoothing occurs, typically set to 15 Å.

Analytical procedures

Map-model correlations for predicted models were calculated after superposition on the corresponding deposited models.

For structures with more than one chain, only the first chain was included for each structure in comparisons.

Side-chain grafting

The grafting procedure was carried out using the *model_building.graft_side_chains* method in Phenix. This function identifies matching residues in two models, then uses the coordinates of atoms in the main-chain for a residue in one model to position the main-chain and side-chain atoms in a matched residue from another. We excluded residues with low confidence (pLDDT < 70, 2% of the total residues), and residues that participate in crystal contacts (any atom in the residue within 6 Å of any atom in a symmetry-related molecule, 23% of all residues).

Evaluation of compatibility of side-chain positions with density maps

We identified side-chain conformations in AlphaFold predictions that were incompatible with corresponding electron density maps as cases where the predicted side-chain conformation matched the density map much more poorly than the deposited model and differed substantially from that found in the corresponding deposited model. To focus on the side-chain conformation separately from the overall location and orientation of each residue, we used the side-chain grafting procedure described above to orient the main-chain of each residue from an AlphaFold prediction to match the main-chain of the corresponding residue in the deposited model. We considered side-chains to differ substantially if the rmsd of side-chain atoms beyond the C_β atom was greater than 1.5 Å.

We then identified incompatible AlphaFold side-chain conformations as those that were highly unlikely ($p < 0.01$) to be as compatible with the density map as the deposited model. This probability was estimated from the uncertainty of density values in each map and the number of independent points sampled by side-chain atomic positions in that map. To obtain the uncertainty of density values, we calculated the rms difference between *Fobs* and *Fcalc* maps obtained from the *phenix.refine (31)* software using the deposited model and crystallographic data to calculate the maps. To estimate the number of independent points sampled by side-chain atomic positions for a particular side-chain, we counted the number of side-chain atoms that could be selected where each atom is separated from all others by at least the resolution of the data.

As an example of this procedure, for the 7vgm example shown in Fig. 3, the mean electron density map value at atoms in the side-chain of residue R32 in 7vgm was 2.8 and the mean density for the side-chain from the AlphaFold model was 0.1 (the map is normalized to have a mean of zero and rms of 1). These side-chains differed by an rmsd of 3.9 Å and the 6 side-chain atoms corresponded to approximately 4 unique positions in the map (4 positions that are each separated from the others by the resolution of the map). The map, adjusted to have a mean of zero and rms of 1, had an estimated uncertainty of 0.8 (based on agreement between the calculated and observed structure factor amplitudes), leading to a probability of $p < 10^{-10}$ that the AlphaFold prediction is actually in better agreement with the map than the deposited model.

Supplementary text

Control experiments and limitations

Our analysis of side-chain conformations is based on the premise that the backbone conformation of the deposited model is largely correct. However, it is possible that the backbone is systematically distorted at residues with incorrect rotamers, as the main chain atom positions might compensate for errors in the side-chain. We checked for this scenario by refitting the side-chains for all 102 structures, and applying a "backrub" correction to the main-chain to correct for these distortions if necessary (*32*). A repeat of our analysis, skipping the 4% of side-chains where a backrub correction was applied (C_β shift (*32*) of more than 0.2 Å), yielded very similar results, with 18% of residues differing in side-chain orientation and again 7% overall clearly incompatible with experimental data.

We also checked for the possibility that backbone conformations might differ in the two models for some residues, making the grafting procedure inappropriate. We repeated our analysis, removing all residues where the Ramachandran angles differed in the two structures by more than 30^o (10% of all residues). Once again, the results were similar, with 17% of residues differing in side-chain orientation and 7% overall clearly incompatible with experimental data.

Our test set (102 for most analyses, 215 for some) is a small fraction of those in the entire PDB, so it could be useful to analyze a larger, more representative set. Most of the residues in our analysis had high confidence, with 86% having pLDDT values above 90, 10% from 80 to 90, 2% from 70 to 80 and 2% under 70. In contrast, in the AlphaFold prediction of the human proteome (*25*), only 38% of residues had pLDDT values above 90, and 42% were under 70. The small fraction of residues with predictions under 80 may lead to some uncertainty in the error estimates for moderate and low-confidence predictions in Table I. The median rmsd between AlphaFold predictions and deposited models in the PDB in our analysis (1.0 Å, see Fig. 2C in main text) was considerably lower than that obtained in a large-scale analysis of recent structures by DeepMind(*1*) (2.3 Å for all C_α atoms, 1.5 Å excluding the largest 5% of differences), perhaps due to the high confidence in prediction in our sample.

As we wanted to estimate the accuracy of the 200 million predictions made with the standard version, we did not remove predictions that might be better-predicted with a multimer version of AlphaFold (*33*). For example, PDB entry 7e1d is a domain-swapped dimer (*34*) that was predicted by AlphaFold to be a compact chain.

In some instances, domain-swapping or other incorrect connections between domains resulted in very large differences between predictions and deposited models. Therefore, we attempted to reduce the effect of these outlier structures by quoting median values where possible.

We used a local installation of AlphaFold for our predictions and did not use templates from the PDB in prediction, which could reduce the accuracy of the predicted models. This effect is likely to be small however. We identified 81 models in the AlphaFold database (*9*) that corresponded to the first chains in one of our 102 analyses. The median C_α atom rmsd between our initial predicted models (*19*) and the corresponding chain in the AlphaFold database was just 0.54 Å. The predictions from the AlphaFold database had a median rmsd of 1.15 Å compared to deposited models; our predictions without templates also had a value of 1.15 Å.